78

FORECAST SENSITIVITY OF WAVES AND SUBMESO MOTIONS TO INITIALIZATION STRATEGY AND PBL PHYSICS IN THE STABLE BOUNDARY LAYER

Astrid Suarez*, David R. Stauffer, and Brian Gaudet
The Pennsylvania State University, University Park, PA

1. INTRODUCTION

The study of submeso motions (i.e., fluctuations with periods of minutes to tens of minutes and horizontal scales of ~0.02 to 2.0 km) using numerical weather prediction (NWP) is difficult because the current mesoscale models have limited skill forecasting the timing and frequency of these events; and we lack a systematic verification method for these transient, nonstationary motions. Traditional verification methods assess dynamical systems based on features extracted from the frequency or the time domain, providing only some perspective of the validity of the model. As a result, classical time-dependent, frequency-independent verification strategies, such as the root mean squared error or mean absolute error, can underestimate the predictability of the model due to phase errors. Time-independent, frequency-dependent strategies such as Fourier analysis can overestimate the predictability of the model due to the inaccurate representation of nonstationary, transient features. So in general, feature-based validation techniques may be ineffective for cases characterized by submeso activity.

The wavelet transform bypasses many of these limitations allowing the evaluation of time series in the time-frequency domain and facilitating the detection of dominant modes and events of short duration (Terradellas et al. 2001). The wavelet transform has been used for the verification of dynamical systems through the evaluation of cross-correlation and cross-coherence (e.g., Jiang and Mahadevan 2011). Model verification using these methods, however, is conducted using the wavelet coefficients in the time-frequency domain, which is complicated by significance testing, correlation of neighboring time and scales in the wavelet domain, spurious coherence regions, and the lack of a general verification metric.

Many of these issues can be avoided by using the wavelet transform as a bandpass filter of uniform shape and varying location. This property of the wavelet transform allows it to be used for data filtering or denoising and permits the analysis of frequency-dependent (i.e., scale-dependent) signals in the time domain. In this study, this property of the wavelet transform is explored in the development of a new verification methodology for nondeterministic modes. This new technique is then implemented for the verification of the Weather Research and Forecasting model (WRF; Skamarock et al. 2008) forecasts for real cases characterized by submeso motions.

2. THE ROCK SPRINGS NETWORK AND OBSERVATIONS

A special observing network, deployed at Rock Springs, Pennsylvania (PA), is used to investigate gravity waves over the complex terrain of central PA (Fig 1). The Rock Springs network is located within the Nittany Valley, 20 km southeast of the Allegheny Mts. and adjacent to Tussey Ridge (Fig 1a). The network consists of two SODARs, founded by the Army Research Office (ARO) Defense University Research Instrumentation Program (DURIP), as well as fast response two- and three-dimensional sonic anemometers and thermistor temperature sensors mounted on 2-, 10- and 50-m towers. These instruments are designed primarily for sampling downslope drainage winds and sub-mesoscale motions in the cold pools. The locations of the towers and SODARs are shown in Fig 1b.

Six cases, characterized by submeso activity and gravity waves, are investigated. The suite of cases is observed during the 2011 summer-fall seasons.

3. MODEL CONFIGURATION AND EXPERIMENTS

In this study, the WRF version 3.3 is configured like that in Seaman et al. (2012). It includes four, one-way-nested domains with 12-,

* *Corresponding author address:* Astrid Suarez, 623 Walker Building, Dept. of Meteorology, The Pennsylvania State University, University Park, PA 16802; email: ais5396@psu.edu

4-, 1.33-, and 0.444-km horizontal grid spacing, respectively. Initial and boundary conditions are provided by the NCEP Global Forecast System (GFS) 0.5°x0.5° data every 6 h. The model physics include the Noah land surface model coupled with the Moderate-resolution Imaging Spectroradiometer (MODIS) land use/land cover, the Rapid Radiative Transfer Model long-wave and Dudhia short-wave radiation schemes, and the Kain-Fritsch cumulus parameterization (12-km domain only).Model verification skill is first assessed for three initialization strategies using the Mellor-Yamada-Janjic (MYJ; Janjic 1990, 1996, 2002) planetary boundary layer (PBL) scheme for six case studies. The initialization experiments include a 12-h free forecast initialized at 0000 UTC (CTRL), a 24-h forecast initialized 12 h prior to the 0000 UTC verification start time (BSL), and a 12-h forecast preceded by a 12-h four dimensional data assimilation period (FDDA). The FDDA pre-forecast includes analysis nudging to GFS analysis data and observation nudging to WMO data and Rock Springs observations. In addition, the verification skill is assessed for four PBL schemes using three case studies with FDDA initialization. This includes the 1) modified MYJ scheme, 2) Yonsei University scheme (YSU; Hong et al. 2006), 3) the Quasi-normal Scale Elimination scheme (QNSE; Sukoriansky et al. 2005), and 4) the Mellor-Yamada-Nakanishi-Niino scheme (MYNN; Nakanishi and Niino 2004).

4. VERIFICATION METHODOLOGTY

The wavelet transform is employed in the development and implementation of a new verification strategy for nondeterministic modes. Deterministic and nondeterministic modes are assessed following the Gaudet et al. (2008) spectral decomposition analysis, in which fluctuations with periods less than 2 h are considered stochastic and nondeterministic. The deterministic verification is conducted for 2-h filtered data using standard mean absolute error (MAE) and mean error (ME). The nondeterministic verification procedure is as follows:

1. ***Decompose*** the signal into its wavelet coefficients using the continuous wavelet transform (CWT), given by

$$W_n(s) = \sum_{n'=0}^{N-1} x_{n'} \psi^* \left[(n' - n) \frac{\delta t}{s} \right] \qquad (1)$$

where s is the scale, n is the translation parameter, δt is the timestep, and ψ^* is the complex conjugate of a scaled and translated Morlet wavelet, given by

$$\psi_0(\eta) = \pi^{-1/4} e^{i\omega_0 \eta} e^{-\frac{1}{2}\eta^2} \qquad (2)$$

where ω_0 is the base frequency.

2. ***Reconstruct*** the time-amplitude series at each Morlet scale independently using

$$x_n = \frac{\delta j \, \delta t^{1/2}}{C_\delta \psi_0(0)} \sum_{j=0}^{J} \frac{\Re\{W_n(s_j)\}}{s_j^{1/2}} \qquad (3)$$

where C_δ and δ_j are wavelet-specific factors (0.4875 and 0.776 for the Morlet wavelet), and j is a scale index. *(Eq. 3 is a bandpass filter of uniform shape and varying location and width with a known response function given by the sum of its scales).*

3. ***Detect*** positive oscillations with amplitudes greater than the instrument precision (e.g., 0.01 K for the thermistors and 0.01 m s^{-1} for the sonic anemometers) for all the frequency-dependent time series.

4. ***Bin*** the retrieved amplitudes to create observed and forecasted distributions of the fluctuations

5. ***Compute Statistics***, fractional relative error (*FRE*) and mean relative error (*MRE*), using the frequency-dependent amplitude distributions. The *FRE* is given by

$$FRE_s^A = \frac{NF_s^A - NO_s^A}{NO_s} \qquad (4)$$

where *A* refers to the amplitude bin, s refers to the scale, and *NF* and *NO* represent the number of forecasted and observed fluctuations, respectively. The *FRE* is selected over the relative error in order to avoid dividing by zero for scales where no oscillations are observed within a particular amplitude bin. The *MRE* is given by

$$MRE_s^A = \frac{1}{N} \sum_{n=1}^{N} \left(\frac{1}{C} \sum_{c=1}^{C} FRE_{s,c}^A \right). \qquad (5)$$

and it is used to summarize information over multiple sites *(N)* and/or cases *(C)*. The *MRE* can be either positive or negative. Large magnitudes of *MRE* imply that the model predictions are not able to capture the

variability of the observed time series at the correct frequency (scale) and/or with the correct amplitude. Positive (negative) *MRE* values indicate the over-prediction (under-prediction) of the number of fluctuations with amplitudes and scales equal to those observed.

The sum of mean absolute relative error (*SMARE*) over all sites and cases is computed for each set of experiments. The *SMARE* is defined as

$$SMARE = \sum_{a=1}^{A}\left(\frac{1}{N}\sum_{n=1}^{N}\left[\frac{1}{C}\sum_{c=1}^{C}\left|FRE_{s,C}^{A}\right|\right]\right). \quad (6)$$

and it is a measurement of the total error. The uncertainty of the *SMARE* is estimated using the standard error, σ, of the *FRE*

$$\sigma = \frac{std\,(FRE_{s,C}^{A})}{\sqrt{N}}. \quad (7)$$

5. RESULTS FOR DETERMINISTIC STATISTICAL ANALSYSIS

Figure 2 shows time series and 10-h means of deterministic, 2-m temperature and wind speed MAEs for the initialization strategies experiments and PBL parameterization experiments. FDDA has some advantages over CTRL and BSL for temperature predictions (Fig 2a). FDDA reduces the 10-h mean MAE by 0.6 and 0.8 K compared to CTRL and BSL respectively, and produces better initial conditions at 0000 UTC. There is little sensitivity to initialization strategy for wind speed predictions (Fig 2b), and wind errors are less than 1.2 m s^{-1}.

For PBL parameterization experiments, MYJ, MYNN, and YSU produce very similar temperature MAEs over the evaluation period while QNSE produces large errors due to a cold bias (Fig 2c). The QNSE produces forecasts that are consistently 2-3 K too low (not shown). There is little sensitivity of wind speed predictions to choice of PBL physics(Fig 2d). However, the deterministic, wind-speed MAEs for all cases are already small (<1.0 m s^{-1}).

6. RESULTS FOR NONDETERMINISTIC STATISTICAL ANALSYSIS

Nondeterministic, temperature MREs for all the initialization experiments are presented in Fig 3. For these cases, the model underestimates small amplitude fluctuations with periods less than 6 min by nearly 100 %. This result is expected since the model is designed to filter small-amplitude, high-frequency fluctuations. The WRF model, however, overestimates the number of small amplitude fluctuations with periods greater than 22 min at the expense of producing fluctuations of larger amplitudes. This result indicates that WRF produces forecasts that are too smooth even for longerperiod fluctuations (in the submeso and meso-gamma range), where better model skill is expected. Similar results are obtained for wind speed MREs and for all PBL physics experiments.

The SMAREs for the initialization experiments are presented for all amplitude bins (Fig. 4a, c) to illustrate the total error of the forecasts and for amplitudes greater than 0.1 (Fig. 4b, d) to illustrate the effect of small amplitude fluctuations on forecast skills. For temperature and wind speed forecasts, much of the variability among experiments for small scales (Fourier periods) are related to fluctuations with amplitudes less than 0.1 K (compare Fig 4 a and b). FDDA appears to show some advantage forecasting the temperature and wind speed variability for periods greater than 22 and 43 min respectively over CTRL (Fig 4 b, d).

For PBL parameterization experiments, temperature and wind speed SMAREs are presented in Fig 5. These experiments also exhibit large variability at high-frequency scales that are associated with small amplitude fluctuations. QNSE better captures the variability of nondeterministic temperature modes with periods > 22 min versus other parameterizations. *TKE*-based schemes (MYJ, MYNN and QNSE) have some advantage over YSU for nondeterministic temperature modes. The limited sensitivity of deterministic and nondeterministic wind speed to PBL option suggests that the parameterizations may be very similar and not a large contributing factor to the predicted wind speed variability.

7. CONCLUSION

The new non-deterministic scale evaluation permits the verification of the submeso variability independent of time and phase error but accounting for the scale and amplitude of the fluctuations. Following expectation, the model completely misses small-period, small-amplitude fluctuations by almost 100 %. However, the model also underestimates the amplitude of fluctuations with periods of submeso and meso-gamma

scales, where the model could better resolve these features. Nevertheless, the model error at these larger scales is small.

For initialization experiments, the FDDA improves the deterministic temperature errors and biases from GFS initialized experiments, while resolving some of the observed variability of nondeterministic predictions. For PBL parameterization experiments, MYJ forecasts temperature and wind fluctuations with wavelength and amplitude closer to observed than YSU and MYNN, and without the large temperature bias of the QNSE scheme.

Further testing of this technique over a larger range of cases, should be implemented in order to understand the source of the amplitude biases over all scales. This study illustrates the need for a combined, deterministic and non-deterministic verification strategy for the study of the SBL.

8. REFERENCES

Gaudet, B.J., N.L. Seam an, D.R. Stauffer, S. Richardson, L. Mahrt and J.C. Wyngaard, 2008: Verification of WRF-predicted mesogamma-scale spectra in the SBL using a high-frequency filter decomposition. Preprints, *9th WRF Users' Workshop,* Boulder, CO, NCAR/MMM, P8.1

Hong, S.Y, J. Dudhia, and S.H. Chen, 2004: A revised approach to ice microphysical processes for the bulk parameterization of clouds and precipitation. *Monthly Weather Review*, 132, 103-120.

Janjic, Z.I., 1990: The step-mountain coordinate: Physical package. *Monthly Weather Review*, 49, 1831-1844.

_____, 1996: The surface layer in the NCEP Eta Model, 11th Conference on Numerical Weather Prediction, Norfolk, Virginia, 19-23 August, American Meteorological Society.

_____, 2002: Nonsingular implementation of the Mellor-Yamada level 2.5 scheme in the NCEP Meso model, NCEP Office Note, No. 437, 61.

Jiang, X., and S. Mahadevan, 2011: Wavelet spectrum analysis approach to model validation of dynamic systems. *Mechanical System and Signal Processing,* **25,** 575-590.

Nakanishi, M. and H. Niino, 2004: An improved Mellor-Yamada level-3 model with condensation physics: Its design and verification. *Boundary Layer Meteorology*, 112, 1-31.

Skamarock, W.C., J.B. Klemp, J. Dudhia, D.O. Gill, D.M. Barker, W. Wang, and J.G. Powers, 2008: A description of the Advance Research WRF version 3. NCAR Tech Note NCAR/TN-468+STR.

Sukoriansky, S., B. Galpering, and V. Perov, 2005: Application of a new spectral theory of stable stratified turbulence to the atmospheric boundary layer over sea ice. *Boundary-Layer Meteorology*, 117, 231-257.

Terradellas, E., G. Morales, J. Cuxart, and C. Yague, 2001: Wavelet method: Application to the study of the stable atmospheric boundary layer under non-stationary conditions. *Dynamics of Atmospheres and Oceans*, **34**, 225-244.

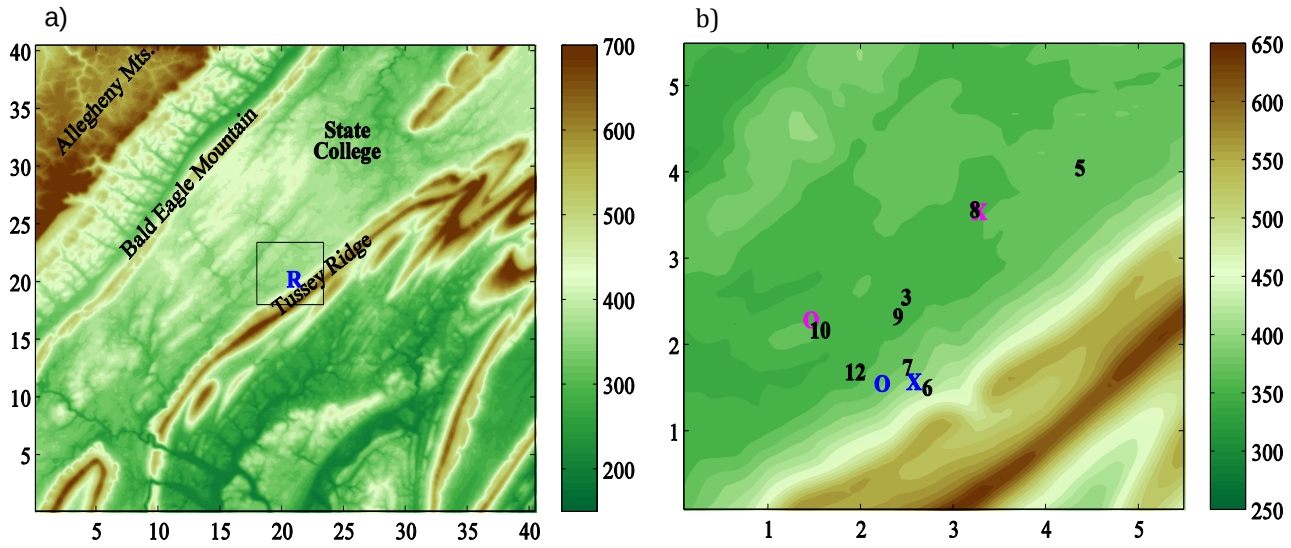

Figure 1. High-resolution (90-m) terrain elevation (m MSL, colored according to scale) for (a) a 40 km by 40 km region containing the Rock Springs network (R) and major topographical features and (b) a 5 km by 5 km region denoted by the black square in a) showing the distribution of instrumented towers and SODARs. X and O represent the locations of SODAR 2028 and 2027 respectively before (blue) and after (magenta) 29 September 2011, respectively.

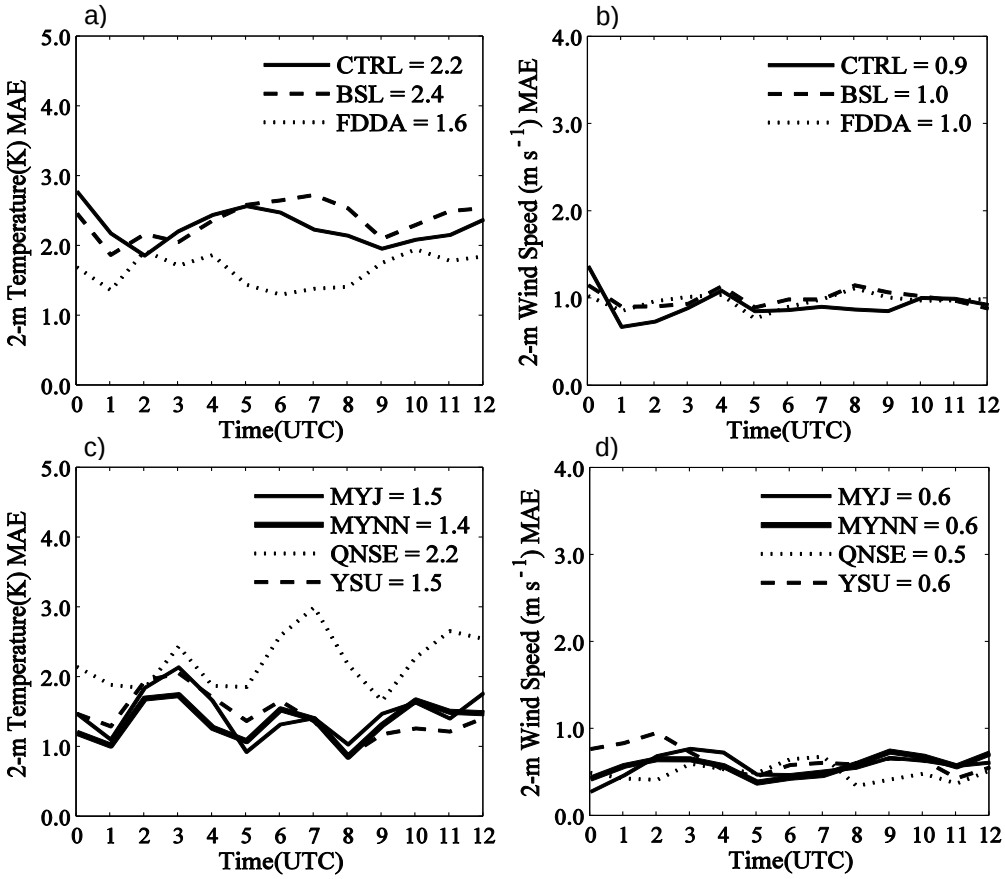

Figure 2. Six-cases MAE of 2-h filtered temperature and wind speed for initialization strategy experiments (a and b) and three-cases MAE of 2-h filtered temperature and wind speed for PBL parameterization experiments (c and d).

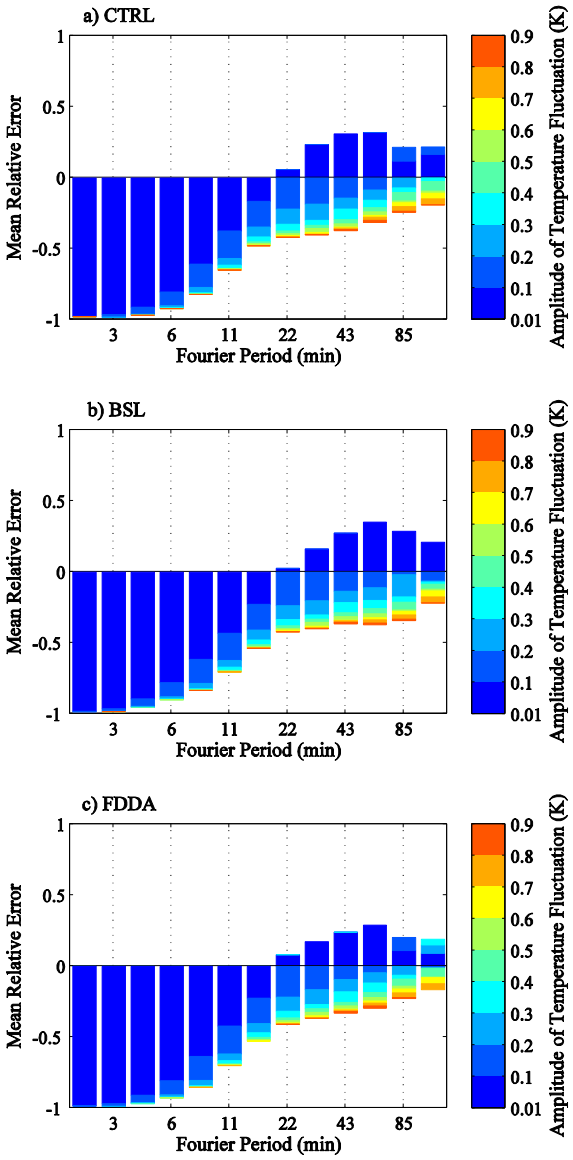

Figure 3. Six-case, temperature MREs for CTRL, BSL and FDDA presented as a function of the equivalent Fourier period (min) and amplitude bin (every 0.1 K; shaded according to scale). Stacked bars represent the total contribution of each amplitude bin error at each period to the total MRE. Negative values indicate the underestimation of the observed variability, while positive values indicate the overestimation of the observed variability.

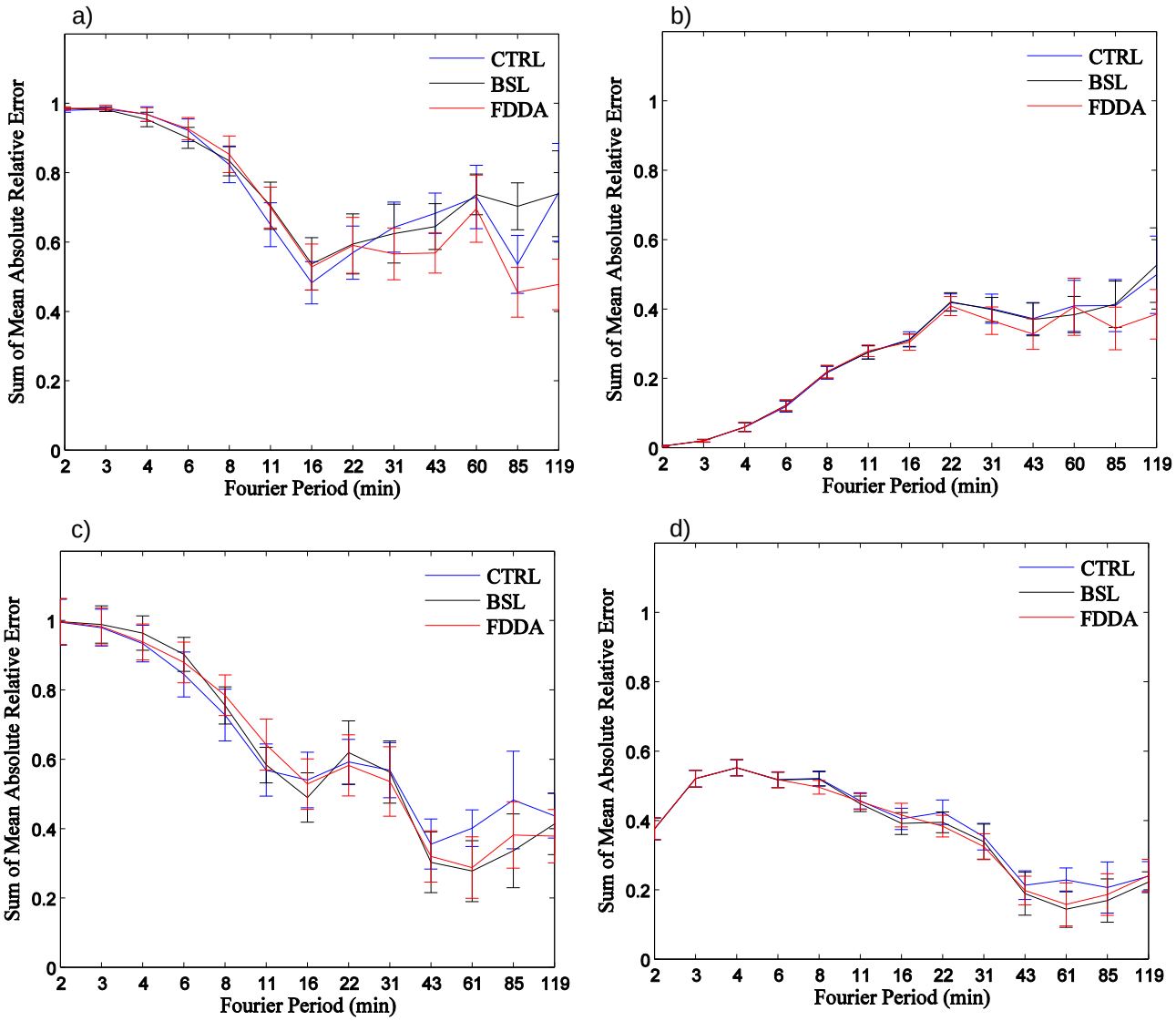

Figure 4. Six-cases, temperature (a and b) and wind speed (c and d) SMARE over all amplitudes (a and c) and 0.1-0.9 K and 0.1-0.9 m s^{-1} temperature and wind speed amplitude range, respectively, (b and d) for initialization-strategy experiments.

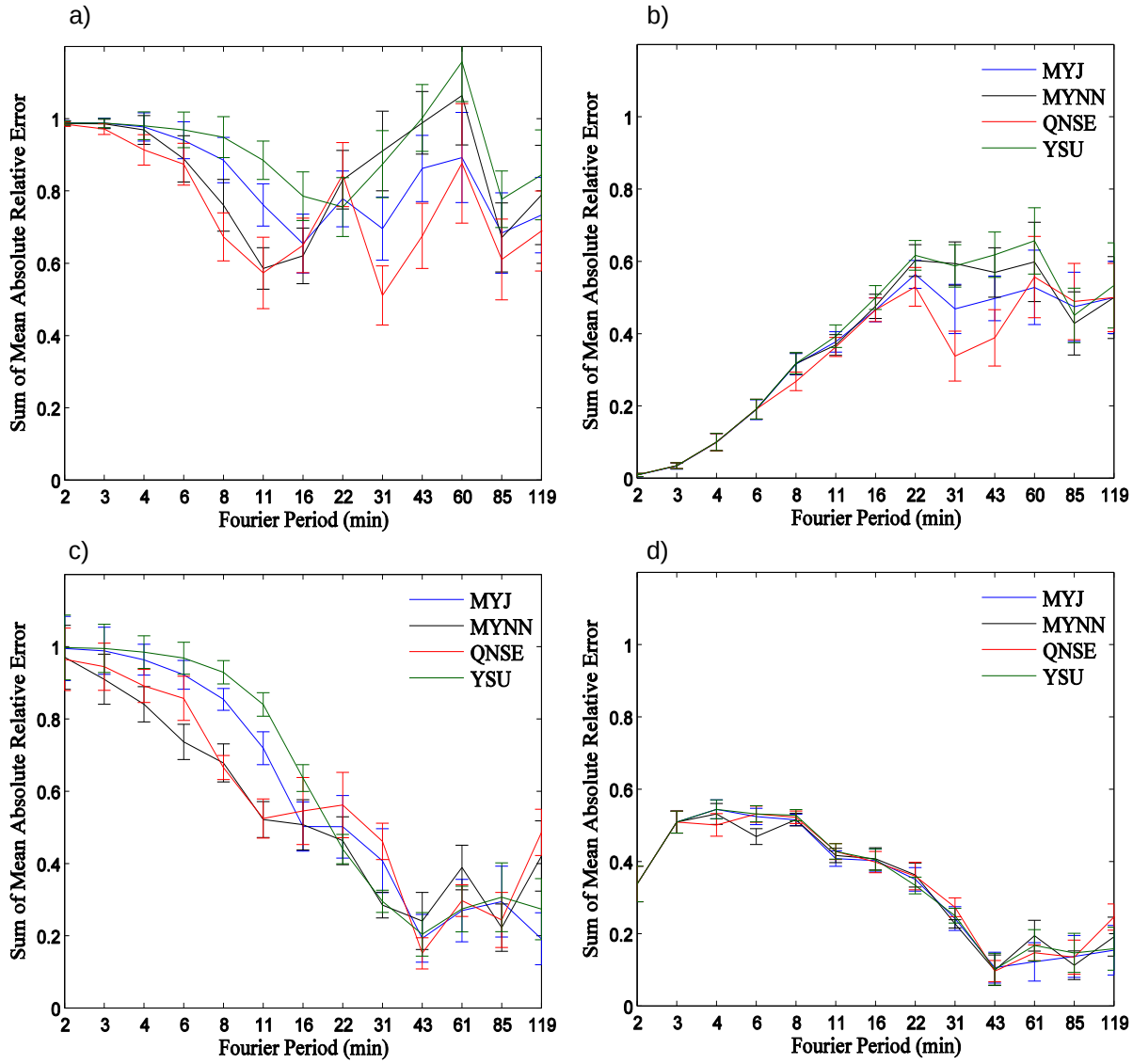

Figure 5. Three-cases, temperature (a and b) and wind speed (c and d) SMARE over all amplitudes (a and c) and 0.1-0.9 K and 0.1-0.9 m s^{-1} temperature and wind speed amplitude range, respectively, (b and d) for PBL-parameterization experiments.